NASA Technical Memorandum 80104

A VECTOR-CONTINUOUS LOADING CONCEPT FOR AERODYNAMIC PANEL METHODS

William B. Kemp, Jr.

May 1979

National Aeronautics and
Space Administration

Langley Research Center
Hampton, Virginia 23665

1 Report No	2 Government Accession No	3 Recipient's Catalog No
NASA TM-80104		

4 Title and Subtitle	5 Report Date
A VECTOR-CONTINUOUS LOADING CONCEPT FOR AERODYNAMIC PANEL METHODS	May 1979
	6 Performing Organization Code
7 Author(s)	8 Performing Organization Report No
William B. Kemp, Jr.	
9 Performing Organization Name and Address	10 Work Unit No
NASA Langley Research Center Hampton, VA 23665	505-06-53-01
	11 Contract or Grant No
	13 Type of Report and Period Covered
12 Sponsoring Agency Name and Address	Technical Memorandum
National Aeronautics and Space Administration Washington, DC 20546	14 Sponsoring Agency Code

15 Supplementary Notes

16 Abstract

A new approach to the reduction of discretization errors in aerodynamic panel methods is introduced. The approach is based on preventing the occurrence of induced velocity singularities at panel slope discontinuities by maintaining continuity of the velocity jump vector across the panels. The approach has been implemented in a two-dimensional incompressible panel method formulation and evaluated by application to several external and internal flow problems. The method is shown to exhibit a second order accuracy trend and to produce smaller errors with velocity component boundary conditions imposed on the real flow than with equipotential boundary conditions imposed on the imaginary flow behind the panels. For flows around airfoil sections with either sharp or blunt trailing edges, the method gives excellent agreement with results from a well developed finite difference method. The method is generally well behaved and is essentially insensitive to irregularities in panel size distribution.

17 Key Words (Suggested by Author(s))	18 Distribution Statement
Potential Flow Surface Panel Method Aerodynamic Influence Method Green's Identity Vector Continuity	UNCLASSIFIED - UNLIMITED STAR Category: 02

19 Security Classif (of this report)	20 Security Classif (of this page)	21 No of Pages	22 Price*
UNCLASSIFIED	UNCLASSIFIED	37	$4.50

* For sale by the National Technical Information Service, Springfield, Virginia 22161

A VECTOR-CONTINUOUS LOADING CONCEPT

FOR AERODYNAMIC PANEL METHODS

William B. Kemp, Jr.
NASA Langley Research Center

SUMMARY

A new approach to the reduction of discretization errors in aerodynamic panel methods is introduced. The approach is based on preventing the occurrence of induced velocity singularities at panel slope discontinuities by maintaining continuity of the velocity jump vector across the panels. The approach has been implemented in a two-dimensional incompressible panel method formulation and evaluated by application to several external and internal flow problems. The method is shown to exhibit a second order accuracy trend and to produce smaller errors with velocity component boundary conditions imposed on the real flow than with equipotential boundary conditions imposed on the imaginary flow behind the panels. For flows around airfoil sections with either sharp or blunt trailing edges, the method gives excellent agreement with results from a well developed finite difference method. The method is generally well behaved and is essentially insensitive to irregularities in panel size distribution.

INTRODUCTION

For computation of potential flow over aerodynamic configurations at subsonic and supersonic speeds, linearized aerodynamic influence methods using surface panels have been used for over a decade with reasonable success even with very complex shapes. Much effort has been expended on the development of such methods to minimize discretization errors and problems with solution stability and local ill conditioning. Such problems have rendered many panel method formulations unreliable unless used with considerable finesse.

Recent demonstrations that these problems can be materially reduced by combining both source and vortex (or doublet) loading on each panel have stimulated the development of several formulations using combined panel loading. Several schemes have been utilized to control the relative magnitude of the two loadings on each panel. In reference 1, Bristow used a global least squares minimization of load magnitudes. Maskew and Woodward (ref. 2) related source loading to the symmetric part of the solution and vortex loading to the antisymmetric part. Later, Woodward developed the supersonic "triplet" panel (ref. 3) which related source and vortex loading so as to cancel the velocity discontinuities propagated along Mach lines emanating from

the back side of each panel. A scheme having several attractive features is that first employed by Morino (ref. 4) and extensively studied by Bristow (ref. 5) who referred to it as "Green's identity". In this scheme the source density and vorticity are equated to the local surface normal and tangential perturbation velocities respectively, one of which is prescribed as a result of the local boundary condition. Ideally, the flow on the back side of the panels is unperturbed. In practice, however, discretization errors cause some departure from the ideal Green's identity relationships. The benefits of this scheme for supersonic flow computations have been demonstrated during development of the panel method described in reference 6.

Many benefits of the combined loading schemes noted can be realized using constant source and vortex strengths on each panel. For improved accuracy, several formulations under study at present (see references 5 and 6) include a linear distribution of vorticity (quadratic doublet distribution) to eliminate the discontinuity of vorticity across panel intersections, thereby eliminating discrete trailing line vortices. Hess' study of higher order source distributions described in reference 7 implies, however, that elimination of first order discretization errors would require the addition of linearly varying source loading and curved panels to achieve continuity of both panel slope and loading.

A somewhat different approach to the problem of reducing discretization errors is described in this paper. The concept of a generalized loading vector having source density and vorticity as orthogonal components is introduced. It is shown that if continuity of the loading vector is maintained across the intersection of two flat panels having an arbitrary difference in panel slope, the singularity in induced velocity which usually occurs at panel intersections is eliminated. To implement this concept, overlapping panel loading elements are developed in which the loading vector is quantified at each panel intersection and its magnitude decreases linearly to zero at the opposite ends of the two intersecting panels. These elements are applied along with the Green's identity principle in a panel method formulation for two-dimensional subsonic external or internal flow problems. In order to exploit the generality of the loading vector scheme, the boundary condition is also generalized to a vector form which includes the Neumann and Dirichlet types of boundary condition among the possible cases. The results obtained from this formulation for several widely different types of flow problem are shown and, in some cases, compared with results from other methods.

SYMBOLS

b	projection of panel length on x axis
c	airfoil chord
$c_{\ell,o}$	section lift coefficient at zero angle of attack
$c_{\ell\alpha}$	section lift curve slope per degree
C_p	pressure coefficient
ℓ	panel length

L	loading vector component
N	number of panels
P	arbitrary field point
Δp, Δq	loading vector components normal and parallel, respectively, to panel corner bisector
r	radial distance, or radius of body nose cavity
u,v	perturbation velocity components in x and y directions, respectively
V	velocity magnitude
x,y	cartesian coordinates
α	airfoil angle of attack
γ	vorticity strength
δ	one half the angular change in panel orientation across a panel corner
θ	angular orientation
λ	angular panel orientation, or average orientation of two intersecting panels
ρ	angular specification of velocity vector relative to panel orientation or average panel orientation
σ	source density
$\Delta\phi$	increment in velocity potential on back side of panels between adjacent control points

Subscripts

B	boundary condition
i	control point index
j	loading element index
N	normal
S	loading specification
T	tangential

U	unknown
γ	induced by vorticity loading
σ	induced by source loading
o	unloaded end of panel
1	loaded end of first panel
2	loaded end of second panel
∞	free stream reference

DEVELOPMENT OF PRINCIPLES

Discretization errors in aerodynamic panel methods arise because the boundary conditions are satisfied only at discrete control points and the velocity distribution along the boundary between control points, being responsive primarily to the local panel loading structure, generally departs from the distribution of the exact solution. Even at the control points, errors are induced thereby in those velocity components unconstrained by the boundary condition. The usual approach to minimizing these errors is to increase the order of continuity required in both the loading and the geometry of the panel system. In practice, however, the enforcement of these continuity requirements is sometimes relaxed in ways that are apparently minor but still might allow the existence of singularities in the induced velocity field.

In the present development, we shift our attention away from the order of continuity and focus instead on the prevention of singular induced velocities. For simplicity the development is described for two-dimensional incompressible potential flow but the principles are applicable in three dimensions and compressible flow and might be particularly useful at supersonic speeds.

Singularity Characteristics

It is expedient first to examine the nature of the singularities that require elimination. Consider an isolated flat panel of length ℓ loaded with a source sheet, the density of which varies linearly from zero at one end to σ_1 at the other. Using the coordinate system shown in figure 1 the velocity components induced by this loading at a point $P(x,y)$ are given by

$$u_\sigma = \frac{\sigma_1}{2\pi}\left[\frac{y}{\ell}(\theta_1 - \theta_0) - \frac{x}{\ell}(\log r_1 - \log r_0) - 1\right] \tag{1a}$$

$$v_\sigma = \frac{\sigma_1}{2\pi}\left[\frac{x}{\ell}(\theta_1 - \theta_0) + \frac{y}{\ell}(\log r_1 - \log r_0)\right] \tag{1b}$$

where the subscripts o and 1 refer to the panel ends at the origin and at $x = \ell$ respectively, r is the distance from point P to the panel end and θ is the angle subtended at the panel end from the x axis to point P.

Observe that as P is brought to either end of the panel, the respective $\log r$ term becomes singular. At the unloaded end of the panel, this singularity has a zero coefficient in both equations which prevents the occurrence of an infinite velocity. At the loaded end, however, the u component is dominated by

the singular term $\frac{\sigma_1}{2\pi} \log (0)$. The v component, although discontinuous at this point, remains finite. To summarize, a triangularly loaded source panel induces a singularity at its loaded end characterized by an infinite velocity directed along the plane of the panel, the strength of the singularity being proportional only to the local source density.

If the source loading were replaced by a similarly shaped vortex loading having a vorticity of γ_1 at the loaded end, the induced velocity vectors would simply be rotated 90^0 such that

$$\frac{u_\gamma}{\gamma_1} = \frac{v_\sigma}{\sigma_1} \tag{2a}$$

$$\frac{v_\gamma}{\gamma_1} = \frac{-u_\sigma}{\sigma_1} \tag{2b}$$

The infinite velocity at the loaded end of the vortex panel would then be directed normal to the panel with a singularity strength proportional to the local vorticity.

Singularity Cancellation

The foregoing discussion suggests that, for purposes of cancellation, each induced velocity singularity can be treated as a vector having the direction of the infinite velocity and a magnitude equal to the local strength of the panel loading giving rise to the singularity.

Now let two panels, each having triangular source and vortex loadings, be brought together so that their loaded ends are coincident and an arbitrary change in panel slope occurs across the intersection. Such a pair of panels is illustrated in figure 2. Let the maximum source density and vorticity on the left panel as viewed in the figure be quantified by σ_1 and γ_1 respectively and those on the right panel by σ_2 and γ_2. The four singularity vectors shown on figure 2 indicate the contribution of each of the four loadings to the induced velocity singularity located at the intersection. Cancellation of the singularity is presumed to occur if the vector sum of the four contributions is zero.

The relationships required for cancellation can be written by inspection if the vector contributions are resolved into components along and normal to the bisector of the panel intersection angle. For this purpose, the angle δ is defined as half the angular change in panel orientation across the intersection. The requirements for singularity cancellation are

$$(\gamma_2 - \gamma_1) \cos \delta - (\sigma_1 + \sigma_2) \sin \delta = 0$$

$$(\sigma_1 - \sigma_2) \cos \delta - (\gamma_1 + \gamma_2) \sin \delta = 0$$

When rearranged as follows

$$\gamma_2 - \gamma_1 = (\sigma_1 + \sigma_2) \tan \delta \tag{3a}$$

$$\sigma_1 - \sigma_2 = (\gamma_1 + \gamma_2) \tan \delta \tag{3b}$$

these expressions show that for a given change in panel slope, singularity cancellation requires a discontinuity in vortex loading proportional to the average source strength and a discontinuity in source loading proportional to the average vorticity.

Vector-Continuous Loading

The source density σ at a point on a panel is identically the difference between the velocity components normal to the panel on the opposite sides of the panel. Similarly the vorticity γ is the difference between the tangential velocity components on the two sides. Thus, the velocity jump vector across the panel has the local values of σ and γ as orthogonal components and will be referred to herein as the loading vector. To clarify the sign convention used, the loading vector is taken as the velocity vector on the panel side facing the real flow minus that on the back side facing a fictitious flow. In the sketches accompanying this discussion, the real flow is that above the panels so that a positive source vector points generally upward and a positive vorticity vector points generally to the right.

The sketches in figure 3 illustrate several features of the loading vector concept. As shown in figure 3a, the combination on a single panel of triangular distributions of both source and vortex loading results in a loading vector with a triangular distribution of magnitude but constant direction along the panel. The concept of loading vector continuity across a panel intersection is illustrated in figure 3b. When the loading vector resulting from σ_1 and γ_1 on the first panel is resolved into σ_2 and γ_2 on the second panel, it is clear that loading vector continuity across nonparallel panels requires discontinuous source and vortex strengths. To quantify these discontinuities it is convenient to resolve the loading vector into components parallel and normal to the panel intersection bisector to form the velocity jump components Δq and Δp respectively, as shown in figure 3c. By inspection we can write

$$\Delta p = \gamma_1 \cos \delta + \sigma_1 \sin \delta = \gamma_2 \cos \delta - \sigma_2 \sin \delta \tag{4a}$$

$$\Delta q = \sigma_1 \cos \delta - \gamma_1 \sin \delta = \sigma_2 \cos \delta + \gamma_2 \sin \delta \tag{4b}$$

It is clear that these expressions for loading vector continuity across the panel intersection can be reduced identically to equations (3), the requirements for cancellation of the induced velocity singularity at the intersection. Thus, singularity cancellation is assured simply by maintaining continuity of the loading vector across each panel corner.

The triangular-shaped vector-continuous loading over two intersecting flat panels appears attractive as a basic loading element for a two-dimensional panel method formulation. Although the direction of the loading vector is uniform in each element, the overlapping of two adjacent elements on a single panel as illustrated in figure 3d causes a continuous variation in both direction and magnitude of the loading vector along the panel. Each loading element is characterized completely by the panel geometry and the two velocity jump components Δp and Δq at the corner. After some manipulation equations (4) can be simplified to give

$$\Delta p = \frac{\gamma_1 + \gamma_2}{2 \cos \delta} \tag{5a}$$

$$\Delta q = \frac{\sigma_1 + \sigma_2}{2 \cos \delta} \tag{5b}$$

or can be solved for the individual source and vortex strengths

$$\begin{aligned} \gamma_1 &= \Delta p \cos \delta - \Delta q \sin \delta \\ \gamma_2 &= \Delta p \cos \delta + \Delta q \sin \delta \\ \sigma_1 &= \Delta q \cos \delta + \Delta p \sin \delta \\ \sigma_2 &= \Delta q \cos \delta - \Delta p \sin \delta \end{aligned} \tag{6}$$

The velocity distributions induced on the panel surfaces and their extensions by an isolated vector-continuous loading element having unit Δq strength are illustrated in figure 4a for several panel corner angles. For comparison, figure 4b shows the distributions induced by source-only loading on panels of the same geometry with continuity of source strength over the corner. For coplanar panels ($\tan \delta = 0$) the loadings of both types are identical and both components of velocity are continuous on the panel surfaces. For the noncoplanar cases, the singularity in the v component of velocity and the discontinuity in the u component induced at the panel corner by the continuous source loading are clearly apparent from figure 4b. In contrast, the velocity distributions induced by the vector-continuous loading element, shown in figure 4a, are free of singularities and discontinuities of magnitude and are generally less sensitive to changes in the panel corner angle. Although the distributions shown on figure 4a and 4b are given for Δq and source-only loadings, respectively, the same curves are applicable to Δp and vortex-only loadings by rotating the velocity components in the manner indicated by equations (2).

Generalized Specifications

The vector-continuous loading element has been incorporated into a pilot two-dimensional panel method formulation to evaluate the characteristics of this loading concept. Although a total of four triangular source or vortex distributions are superimposed on each panel, the satisfaction of equations (3a) and (3b) to form the vector-continuous loading element leaves each element with only two remaining degrees of freedom. In the present formulation, one component of the loading vector at each panel corner is specified using the Green's identity principle leaving the other component as an unknown to be solved for by satisfying the boundary conditions.

Considerable flexibility has been built into the formulation to facilitate the evaluation of the present loading concept for a broad range of problem applications. For example, the control point associated with a given panel can be located anywhere on the panel including the panel corner itself. Cancellation of the singularity at the corner has rendered the velocity at that point calculable.

One feature that has been particularly useful is the use of a generalized vector form for specifying both the boundary condition and the specified component of the loading vector. As illustrated in figure 5 the boundary condition is specified at each control point in terms of the magnitude V_B of the total velocity component in the direction given by the angle ρ_B from the panel surface. The boundary condition on the perturbation velocity is then expressed by

$$V_B - V_\infty \cos(\rho_B + \lambda_B) = u \cos(\rho_B + \lambda_B) + v \sin(\rho_B + \lambda_B) \qquad (7)$$

In accordance with the Green's identity principle, the flow on the back side of the panels is presumed to be unperturbed so the loading vector at a panel corner would be equal to the perturbation velocity in the real flow at that point. Because, however, the loading vector constraint is derived from the problem definition just as though it were a boundary condition, it also is specified as a total velocity component with magnitude V_S and angle ρ_S where ρ_S is measured from the Δp axis which is normal to the panel corner bisector. The loading vector is the resultant of the specified component

$$L_S = V_S - V_\infty \cos(\rho_S + \lambda_S) \qquad (8)$$

and an unknown component L_U which is orthogonal to L_S. The aerodynamic influence coefficients are calculated as values of UP_{ij}, VP_{ij}, UQ_{ij}, and VQ_{ij} where UP_{ij} is the u component of the perturbation velocity induced at control point i by a unit Δp loading on element j, etc.

By expressing

$$\Delta p = L_S \cos \rho_S - L_U \sin \rho_S \tag{9a}$$

$$\Delta q = L_S \sin \rho_S + L_U \cos \rho_S \tag{9b}$$

the boundary condition equation (7) can be expanded to the form used for the system of linear equations

$$\begin{aligned}
&\sum_j \Big[(UQ_{ij} \cos \rho_{S,j} - UP_{ij} \sin \rho_{S,j}) \cos (\rho_B + \lambda_B)_i \\
&+ (VQ_{ij} \cos \rho_{S,j} - VP_{ij} \sin \rho_{S,j}) \sin (\rho_B + \lambda_B)_i \Big] L_{U,j} \\
&= V_{B_i} - V_\infty \cos (\rho_B + \lambda_B)_i - \sum_j \Big[(UP_{ij} \cos \rho_{S,j} + UQ_{ij} \sin \rho_{S,j}) \cos (\rho_B + \lambda_B)_i \\
&+ (VP_{ij} \cos \rho_{S,j} + VQ_{ij} \sin \rho_{S,j}) \sin (\rho_B + \lambda_B)_i \Big] L_{S,j}
\end{aligned} \tag{10}$$

Equation (10) is suitable for all control points in problems in which boundary conditions in the form of velocity component specifications are imposed on the real flow side of the panels. Its flexibility allows a mixture of Neumann and Dirichlet boundary conditions and anything in between to be imposed easily. With appropriate modifications to equation (10) the vector-continuous loading element has also been evaluated with boundary conditions imposed on the back side of the panels either in the form of a perturbation velocity component or of the perturbation potential increment between adjacent control points. The aim is to achieve an unperturbed back side flow so that the loading vector constraints can act as boundary conditions on the real flow. The potential increment form requires one less equation than the number of control points so that one equation is available for special purposes such as circulation control.

The present formulation requires that the geometric figure formed by the panels be fully closed and that the vector continuity constraints of equations (3) be imposed at all panel corners. It is possible that some benefits could result from replacing the loading vector continuity conditions with special conditions at certain points where flow singularities would be allowed. In the interest of a thorough evaluation of the vector continuous loading concept, however, such special points have not been used for any of the cases discussed in this paper.

EVALUATION OF METHOD

Special Test Problems

Circular cylinder.- In his classical study of higher order source panels (ref. 7) Hess shows that elimination of first order discretization errors, i.e., those errors proportional to panel length, requires distributions of both source strength and panel slope which are linear on the panels and continuous across panel junctures. The foregoing discussion of vector continuous loading suggests that with combined source and vortex loading, the continuous variation of the loading vector might replace the function of panel curvature thereby allowing the achievement of second order accuracy even with flat panels. To test this hypothesis, several variants of the present formulation were used to calculate the nonlifting flow around a circular cylinder paneled with 20 or 40 panels. Circulation control was achieved by specifying a tangential constraint on the loading vector at the downstream stagnation point. The results are shown in figure 6 in the form of root mean square errors in either vorticity or tangential velocity at panel midpoints and panel corners. The errors were determined as differences between the panel method and exact solutions expressed relative to the exact solution values.

The results in the upper plot of each part of figure 6 were obtained with zero normal velocity boundary conditions and those on the lower plot with constant internal potential boundary conditions. The formulation of figure 6a used vector-continuous loading elements with the boundary conditions imposed on control points located at the panel corners. That of figure 6b differed only in that the control points were at the panel midpoints, with the loading constraints still being imposed at the panel corners. Observe that the abscissa in both figures (6a and 6b) is the square of the inverse number of panels. The linear trends obtained for both the vorticity and tangential velocity errors confirm that second order accuracy was indeed achieved.

With zero normal velocity boundary conditions the tangential velocity error is zero at the control points (panel corners in figure 6a and mid points in 6b). A similar error cancellation was noted by Hess in reference 7 at the mid points of flat constant strength source panels on a circular cylinder. Even between control points, however, the present results show tangential velocity errors that are significantly smaller than the errors in vorticity. Apparently, with zero normal velocity boundary conditions, most of the discretization error appears as a perturbation in the fictitious interior flow rather than distorting the real exterior flow.

The constant internal potential boundary condition caused much larger tangential velocity errors while suppressing the vorticity error at the panel corners as shown on the lower plots of figures 6a and 6b. With this boundary condition, little effect of moving the control points was observed except that a low level error, alternating in sign at successive panel corners, appeared when the control points were at the panel corners. The total r.m.s. errors are shown by flagged symbols on the lower plot of figure 6a. The

corresponding unflagged symbols (and connecting lines) show the remaining errors after removing the alternating component. This problem is an example of several observations which imply that the vector-continuous panel formulation is not as well behaved with control points at the panel corners as with control points at mid-panel locations.

The results shown in figure 6c illustrate the effect of replacing the vector continuity conditions of equations (3) with the more conventional continuous vorticity and continuous source strength. Otherwise, the formulation is the same as that of figure 6b, having linearly varying source and vorticity loadings on each panel with the loading component specification at panel corners and the boundary condition imposed at panel midpoints. Note that the abscissa in figure 6c is simply the inverse number of panels so that a linear trend indicates first order accuracy.

With zero normal velocity boundary conditions the vorticity errors resulting from this formulation show a first order trend. The errors in tangential velocity at the control points are very small and appear to follow a nearly second order trend. The tangential velocity errors away from the control points, although not shown here, were found to vary markedly along the panels and did, in fact, become singular at the corners for this case. With constant internal potential boundary conditions the results show a second order trend in vorticity errors but a first order trend in tangential velocity errors. Bristow and Grose (ref. 5) applied flat panels with linear vorticity but constant source strength to the circular cylinder problem and noted a similar change in the trend of panel midpoint vorticity error from first to second order as the boundary condition was changed from zero normal velocity to constant internal potential. They did not show the tangential velocity errors, however, nor the vorticity error at panel corners.

It is presumed that with the conventional constraints on source and vorticity continuity, the appearance of second order accuracy in certain combinations of boundary condition and result quantity is due to first order error cancellation arising from the symmetry of the circular cylinder problem. With the vector-continuous formulation, however, elimination of first order errors is achieved in a more general sense.

Concave nose body.- In his accuracy study of source panels (ref. 7) Hess used several test problems for which exact solutions are known and which appeared particularly sensitive to deficiencies in panel formulation. Two of the same problems were used in the present study to assess the effect of combined loadings and vector continuity. The first such problem is calculation of the flow over a semiinfinite body having a semicircular cavity in the nose. The body was derived analytically in reference 8 as the shape of the free streamlines springing from the ends of a semicircular source sheet. In the present study the body was terminated at a length of about eight nose radii by four panels oriented approximately normal to the local streamlines on which the boundary condition of zero tangential velocity was imposed. A zero normal velocity boundary condition was used at all other points.

Figure 7 illustrates the body geometry and compares the exact analytic solution for tangential velocity in the nose cavity with results from several panel formulations using panel lengths on the cavity surface corresponding to 5^{0} of arc. The results using flat constant strength source panels are in essential agreement with those given in reference 7 for the same paneling and show an extensive region of the cavity in which the tangential velocity is in the opposite direction from that of the exact solution. The remaining three formulations shown on figure 7 all used source and vorticity loadings combined according to the Green's identity scheme and all gave results much closer to the exact solution than the constant strength source panels. Although the benefits of combined loading are sometimes attributed to a reduction in discretization error commensurate with the reduced magnitude of panel loading, it should be noted that the peak loading magnitude was reduced by a factor of only about three from the constant source panel case to the constant combined loading case on figure 7 but the tangential velocity error was reduced by a much larger factor. It should be noted also that the results given for the constant strength, combined load case were obtained in an unorthodox manner because the straightforward solution for vorticity strengths was poorly behaved. Instead, an iterative procedure was used in which the vorticity was prescribed from the calculated tangential velocity and the linear equations solved for source strengths.

The accuracy of the various methods can be compared more readily by referring to Table I which lists the error in velocity in the vicinity of the stagnation point, expressed relative to the exact velocity. The results from reference 7 for source loadings only show that the relative error of -2 obtained with flat constant strength panels could be reduced somewhat with either curved panels or linear source loading. The error level achieved with both curved panels and linear source loading was too small to read from the figure in reference 7 but appeared to be better than the level of .04 obtained in the present study with combined constant strength source and vorticity loading. The present results show that little improvement was gained from including linear loadings when the conventional source and vorticity continuity constraints were used. With the vector-continuous formulation, however, the relative error was reduced to .0023.

In figure 8 the surface tangential velocity is plotted against the lateral coordinate y to compare the various methods in the highly curved region just outboard of the semicircular cavity. The analytic solution shows a tangential velocity singularity at the end of the semicircle and a velocity minimum in close proximity to the singularity. The symbols show the tangential velocity at the panel midpoints calculated by each method and illustrate the coarseness of the paneling used in this highly curved region. The vector-continuous formulation gave excellent agreement with the exact solution except for one point at the velocity minimum where the error, although noticeable, is less than that from the other methods. It is interesting to compare the results of the various methods in the vicinity of the velocity singularity. Both the vector continuous panels and those with constant strength combined loading show a pronounced velocity peak at the singularity location. Even the constant strength source panels give a weak indication of a velocity peak. With linear combined loading and the conventional source and vorticity continuity, however,

the results show a smooth distribution of tangential velocity with no indication that the velocity peak should exist.

Closed end duct.- The second problem used to compare the present formulation with those studied in reference 7 is the flow into a straight duct closed at one end with a semicircular shape. The geometry is illustrated by the sketch given in Table II. The tabulated results show the average streamwise velocity calculated at a station spanning the duct at the beginning of the rounded end. The results given in reference 7 for source panels show that the flat constant strength panels allowed flow leakage through the closure at about seven percent of stream velocity and that the use of curved panels was particularly important in reducing the leakage.

This problem was adapted to the present formulation by imposing a zero tangential velocity boundary condition on panels placed across the open end of the duct. The panel spacing at the closed end again subtended 5^{o} of arc. With flat constant strength source panels, the leakage velocity was only slightly greater than the corresponding value from reference 7 as shown in Table II. The use of combined loading with a Green's identity constraint completely eliminated the leakage even for flat constant strength panels. To understand this result, consider that under the Green's identity concept, the exact solution to the closed end duct problem consists of a uniform stagnant internal flow field and a uniform external flow having the free stream velocity. The velocity jump vector (loading vector) at any point on the boundary is, therefore, simply the opposite of the free stream velocity vector. On a flat panel, this loading vector resolves into constant strength source and vorticity components. Thus, the flat panel with constant strength combined loading offers all of the capability needed to reproduce the exact solution.

When the order of the panel loading is increased by introducing linear loading constrained by source and vorticity continuity, the loading vector is forced to change direction at any corner involving a change in panel slope. Because this feature is not compatible with the exact solution, flow distortions are introduced which result in leakage of about one percent of free stream velocity. The vector continuity constraint however, is clearly compatible with the uniform velocity jump vector on the boundary of the exact solution. The solution obtained with the vector-continuous formulation confirmed that the leakage was completely eliminated.

Variable area duct.- A more representative internal flow problem is the flow through the variable area duct illustrated in figure 9. The geometry, as shown in the upper part of the figure, corresponds to a reduction in duct width by a factor of one quarter from the entrance to the exit ends. The longitudinal spacing of the panel end points shown by the tick marks reduces suddenly by a factor of one half partway along the duct walls. Boundary conditions were imposed as zero normal velocity on the upper and lower walls, zero tangential velocity on the panels spanning the small exit end of the duct, and a velocity component of 0.25 normal to the panels spanning the large entrance end. If these boundary conditions were satisfied exactly, the average velocity at the duct exit station would be unity. Panel loading constraints

were derived from the boundary conditions using the assumption of a uniform exterior flow having unit velocity in the direction of the duct axis. At the intersections of the walls with the entrance station, the loading constraint was based on the wall flow tangency condition although the entrance velocity specification could have been used instead.

In the lower part of figure 9 the distribution of tangential velocity along the duct walls obtained with the present vector continuous formulation is compared with a solution using constant strength combined loading panels which, in this case, was a direct solution without iteration. The vector continuous formulation produced a smooth distribution with an exit velocity very close to unity. The constant strength panels, on the other hand, yielded excessive exit velocity and an oscillatory distribution. The oscillation is apparently associated with the abrupt change in panel size because it was not apparent in another direct solution (not shown) using the smaller constant strength panels over the entire duct length. The exit velocity was still excessive, however.

The error in average exit velocity is given in Table III for several formulations. The first three cases show a successive reduction in error magnitude as the panel load distribution is refined from constant through linear with continuous source and vorticity to linear with vector continuity. The last four cases used vector continuous loading but with the equipotential boundary condition imposed on the imaginary back side flow. The loading constraints specified at the panel corners then serve as effective boundary conditions on the real internal flow. The results in Table III show that when the extra equation made available by this boundary condition scheme was used to constrain the total circulation to zero, the exit velocity error was of the same order as that produced by the simple constant strength panels. The sign of the error was positive or negative depending on whether the equipotential boundary condition was imposed at panel midpoints or corners. For the present duct flow problem the total circulation constraint is redundant because the tangential loading specification on the exit face panels provides a similar constraint. Use of the extra equation to constrain the total source strength to zero gave more accurate solutions but the exit velocity errors were still three to four times that resulting from velocity boundary conditions imposed directly on the real flow.

Use of the back side equipotential boundary condition apparently permits discretization errors in the back side flow to be transferred into the real flow as boundary condition errors which can combine adversely with the discretization errors in the real flow. It should be noted that other researchers have found this form of boundary condition to be beneficial (e.g., refs. 5 and 6). It is postulated that the benefit is associated with the velocity averaging property of the equipotential specification so that induced velocity anomalies lying between control points are accounted for. By minimizing such induced velocity anomalies, the vector-continuous formulation reduces the benefit of the equipotential boundary condition but the adverse effects of inexact satisfaction of the intended real flow boundary conditions remain.

Airfoil Analysis Applications

In using a surface panel method for computation of the flow around airfoils it is particularly important to model the trailing edge region in such a way that the Kutta condition can be satisfied with accuracy. The effect of modeling deficiencies is particularly apparent on airfoils having significant camber near the trailing edge and on those having finite trailing edge thickness. The NASA LS(1)-0417 airfoil section has both of these properties and therefore was selected for the present study. The coordinates of the LS(1)-0417 (formerly known as the GA(W)-1) section are given in reference 9.

Sharp trailing edge.- The application of the present vector-continuous panel method to a sharp trailing edge airfoil is discussed first. The airfoil section used for this purpose was formed by removing a thickness increment proportional to x/c from the LS(1)-0417 section while leaving the mean camber line unchanged. In the present study the coordinates defining the airfoil section were used directly as the coordinates of panel corner points without any attempt to smooth the panel size distribution. The basic formulation was that which gave the best combination of accuracy and solution reliability for the problems described in the foregoing sections. In this formulation external flow tangency boundary conditions were imposed at panel midpoints. For this purpose the local surface slope was represented simply as the panel slope. Loading vector components specified at the panel corners corresponded to a zero external velocity component along the corner bisector.

This basic formulation was implemented over the entire airfoil surface except in the immediate vicinity of the trailing edge where several different modifications were tried as means of achieving circulation control so as to satisfy the Kutta condition. In the context of computation methods in which the surface boundary condition is enforced only at discrete points, the existence or absence of a flow singularity at the trailing edge is not a suitable indication of satisfaction of the Kutta condition. For example, the vector continuity condition used in the present formulation prevents the occurrence of singular velocities anywhere. As an alternative, the Kutta condition is generally considered to be satisfied when there is no flow normal to the trailing edge bisector at (or very near) the trailing edge location. Because the reliability of even this alternative indicator is subject to details of the particular loading scheme used, the Kutta condition has been implemented in some methods in terms of a relationship between upper and lower surface panel loadings to cause a zero net vorticity at the trailing edge.

With the present formulation, it is possible to specify a loading component at the trailing edge which corresponds (assuming unperturbed internal flow) to the Kutta condition of zero velocity normal to the trailing edge bisector. This is accomplished by setting $V_S = 0$ and $\rho_S = 0$ in equation (8). It should be noted in passing that equations (9a) and (5a) show that with this loading specification, the net vorticity at the trailing edge is not precisely zero unless the trailing edge is perfectly cusped ($\delta = 90^o$).

The trailing edge loading specification corresponding to the Kutta condition has been used with several trailing edge paneling arrangements. three of which are shown in figure 10. Paneling details over the last five percent chord are shown on the left side of the figure. Panel corners are indicated by crosses and control points by circles. On the right side, the pressure coefficients calculated at the control points over the last 17 percent of the airfoil at zero angle of attack are compared with inviscid results for the same airfoil calculated by the transonic finite difference method of reference 10 for a Mach number of 0.01. The lift coefficient at zero angle of attack and the lift curve slope evaluated from zero to four degrees angle of attack by each method are also shown. The lift coefficient for the panel method was determined from the vorticity integral summed over all panels.

In panel model S-1 on figure 10, all panel sizes corresponded to the basic airfoil coordinate spacing which was 0.025 chordwise over the rear part of the airfoil. It was observed during trials with this model that the calculated lift coefficient was sensitive to the relative location of the upper and lower surface control points nearest the trailing edge. Apparently the flow direction leaving the airfoil was weighted most heavily by the flow direction enforced at the control point nearest the trailing edge. It would seem appropriate, therefore, to model a sharp trailing edge such that the nearby control points are located symmetrically with respect to the trailing edge bisector. The panel models shown in figure 10 maintained this symmetry in the last 0.025 chord region. The value of $c_{\ell,o}$ produced by panel model S-1 was higher by .0008 than that obtained when the last upper and lower control points were at the same chordwise location. The sensitivity to control point asymmetry was observed to be greater for airfoils having a larger included trailing edge angle.

The results shown for panel model S-1 indicate a significantly smaller value of $c_{\ell,o}$ and a slightly smaller lift curve slope than those given by the finite difference method. In this panel model the Kutta condition is used to constrain only the velocity jump between the internal and external flows at the trailing edge. Absolute constraints on the external flow direction are imposed only at the control points. Although the trailing edge bisector is inclined downward 11.99^{o} from the chord line, a trailing edge flow deflection of only 10.54^{o} resulted from the S-1 panel method.

For panel model S-2, two short panels were added so that the last control points were within about one quarter percent chord of the trailing edge. Care was taken to specify the added panel corner coordinates with sufficient accuracy to prevent altering the panel slopes. The resulting trailing edge flow deflection was 11.09^{o}; the discrepancy between the panel and finite difference values of $c_{\ell,o}$ was reduced and that of the lift curve slope was virtually eliminated.

In panel model S-3, only one short panel was added but its associated control point was located at the trailing edge. With this arrangement, the Kutta condition is imposed directly on the exterior flow and the resulting values of both $c_{\ell,o}$ and lift curve slope agree very closely with those from the finite difference method. The airfoil contour interpolation scheme used in the finite difference method should lead to a slightly higher $c_{\ell,o}$ through its effect on the trailing edge bisector direction.

The effectiveness of using a control point to impose the Kutta condition was further demonstrated by runs to determine the effect of a 1^{o} change in the flow direction specified at the trailing edge. With panel model S-3, the value of $c_{\ell,o}$ changed by .0115 but with model S-1, in which the Kutta condition is implemented only through the loading specification, the change in $c_{\ell,o}$ was less than .0001. A variant of model S-3 in which the extra panel corner was located on the upper surface rather than on the lower surface gave results which were essentially identical to those shown for S-3.

The pressure distributions on the right side of figure 10 show some discrepancies between the panel method and finite difference method results in the last five percent of the chord. None of the panel models appeared particularly superior to the others in this respect. It is noteworthy that although the resolution used in the finite difference method was much finer near the trailing edge than that of the panel method, neither method indicated the existence of a stagnation point. When trailing edge stagnation was enforced by a variant of model S-2 in which orthogonal boundary conditions could be superimposed at the trailing edge, the remaining solution was so distorted as to imply serious incompatibility of constraints.

Blunt trailing edge.- The blunt trailing edge airfoil problem is an anomalous application for a potential flow computation method because the solution desired is that which best approximates a viscous flow having a separated wake. Several approaches have been used to model such a potential flow computation. One approach is to deny the existence of flow in a strip extending downstream from the blunt trailing edge by requiring flow continuity across the strip just as though its upper and lower boundaries were coincident. This approach is used in the finite difference method of reference 10 but does not appear to be applicable to panel methods. An approach which has been used with several panel methods is to allow sufficient net source strength at the airfoil to fill the wake with an irrotational flow. A third approach noted as an option in reference 11, is to add a nonlifting downstream fairing to create a sharp trailing edge. The positive net source approach is used herein.

Three of the blunt trailing edge panel arrangements tried with the present vector-continuous loading method are illustrated in figure 11. In each case, the specified loading components at the upper and lower corners of the blunt trailing edge were based on the assumption of zero flow normal to the upper or lower surface panels. Results from the finite difference method of reference 10 are again included for comparison.

Panel model B-1 resulted from the direct use of the specified airfoil coordinates as panel corners with a control point located at each panel midpoint. The control point on the panel closing the trailing edge was used to impose the Kutta condition on the exterior flow by specifying zero velocity normal to the trailing edge bisector. In panel model B-2, the trailing edge closure was divided into two panels and the associated control points were located at the trailing edge corners where the boundary condition of no flow normal to the upper or lower surface trailing edge panel was applied. Panel model B-3 was identical to B-1 except that the flow direction constraint at the trailing edge was replaced by a requirement that the pressures at the upper and lower trailing edge corners be equal. This requirement was implemented in its full nonlinear form which required that the solution be iterated to convergence.

The lift results from these blunt trailing edge panel models follow a pattern similar to that established by the sharp trailing edge results in that the calculated lift coefficients are too low unless the direction of flow leaving the airfoil is established by one or more control points located at the trailing edge. Panel models B-3 and S-1 both impose a condition corresponding to zero lifting pressure at the trailing edge but do not constrain the trailing edge flow direction and give deficient lift coefficients. Model B-1 can be considered as the blunt trailing edge counterpart of S-3 and the results from both agree reasonably well with those from the finite difference method. The additional trailing edge control point in model B-2 resulted in only a very slight increase in $c_{\ell,o}$ and c_{ℓ_α}.

The pressure distribution over the rear portion of the airfoil calculated using each of the panel models is in good agreement with that from the finite difference method except on the lower surface just ahead of the trailing edge. Again, none of the panel models appeared particularly superior to the others in this respect.

The net source strength in the blunt trailing edge panel method solutions was determined by summing the source density integral over all panels and agreed well with that determined from the average velocity out of the trailing edge. The lift increment representing the downward momentum of this added mass was found to agree well with that determined from the vorticity integral over the trailing edge panel, and amounted to an increment of 0.002 in $c_{\ell,o}$ Because this mass would not be added in a real flow with a separated wake, the corresponding lift increment has been omitted from the panel method results given on figure 10.

The added mass emerging from the blunt trailing edge can be considered to act as a jet flap. In addition to the force resulting directly from the jet momentum, a jet flap causes a lift increment by inducing additional circulation. The two-dimensional jet flap theory of Spence as described in reference 12 was applied to the present problem and indicated that the jet-induced circulation in the blunt trailing edge solutions of figure 10 should cause the lift coefficient to be about 1.7 percent higher than the corresponding sharp trailing edge value. The increase in $c_{\ell,o}$ between the results from panel models S-3 and B-2 agrees well with the predicted jet flap effect but the increase in lift curve slope is not as large as that predicted.

Although the direct contributions of the jet momentum can be identified and removed from the solution, the effects of jet-induced circulation are not accounted for as easily. An attempt was made to suppress this unwanted jet-induced effect by adding the equal wake pressure constraint of panel model B-3 to the control point constraints used in model B-2. The additional loading degree of freedom required was obtained by subdividing the last panels on the upper and lower surfaces rather than the trailing edge panel. This attempt was unsuccessful because although the lifting pressure difference was eliminated at the trailing edge, it was increased in the region just ahead of the trailing edge. The resulting c_{ℓ_α} was unchanged from that of model B-2 but $c_{\ell,o}$ was increased to .577.

Of the blunt trailing edge paneling arrangements tested, model B-1 is judged most suitable for general application. The fact that the trailing edge flow is less rigidly constrained than with model B-3 tends to compensate for the errors introduced by the excess source strength needed to fill the wake with potential flow. In addition, B-1 is the blunt trailing edge model which is most similar in concept to panel model S-3, the preferred model for a sharp trailing edge.

Pressure distribution.- The pressure coefficient distribution on the surface of the LS(1)-0417 airfoil section at zero angle of attack as determined from the present vector-continuous panel method is compared on figure 12 with that from the finite difference method of reference 10. The finite difference solution is shown by the solid line and indicates several local irregularities, particularly between the leading edge and 20 percent chord, which arise because the airfoil coordinates have not been subjected to a very refined smoothing process.

The pressure coefficients from the panel method solution are shown at the control point locations by circle symbols and at the panel corners by crosses. Elimination of velocity singularities at the panel corners by the vector-continuous loading used in the present method has made possible the calculation of pressure coefficient at these points. Figure 12 shows that the panel method results, both at the control points and at the panel corners, are in very good agreement with the finite difference results. In particular, the improved resolution provided by the corner point data allows the pressure irregularities to be defined essentially as well with 75 panels on the airfoil as with the finite difference solution which is given at 160 points on the airfoil surface. Note also that no apparent anomalies are introduced by the abrupt changes in panel size at .05, .20 and .55 chord.

Although the results shown on figure 12 illustrate the usefulness of data evaluated at the panel corners to enhance the resolution obtainable with a given number of panels, it has been observed that the panel corner data are not always suitable for this purpose. In some solutions the corner point data intermesh poorly with data evaluated at the control points in regions where details of the problem formulation have allowed perturbations in the imaginary flow behind the panels to become large. It is suggested that flow data evaluated at panel corners be considered less reliable than those evaluated at the control points until the factors affecting the relative accuracy of these data are better understood.

CONCLUDING REMARKS

A new approach to the reduction of discretization errors in aerodynamic panel methods has been described. The approach is based on preventing the occurrence of induced velocity singularities at panel slope discontinuities by maintaining continuity of the loading vector, which is the velocity vector jump across a panel. Within this concept, the vorticity and source density on a panel are recognized as the loading vector components resolved parallel and normal respectively to the panel surface. The approach has been implemented in a two-dimensional incompressible panel method formulation and evaluated by application to several internal and external flow problems.

When applied to certain problems for which exact solutions are known, the method is shown to exhibit a second order accuracy trend and to produce smaller errors with velocity component boundary conditions imposed on the real flow than with equipotential boundary conditions imposed on the imaginary flow on the back side of the panels. For flows around airfoil sections with either sharp or blunt trailing edges, the method gives excellent agreement with results from a well developed finite difference computation method. The method is generally well behaved and is essentially insensitive to irregularities in panel size distribution.

Although the favorable properties of the vector-continuous loading concept are demonstrated herein only for two-dimensional incompressible applications, it is anticipated that these same properties should lead to a simplification in the panel method formulation required for a given accuracy in three-dimensional solutions and a lessening of problems with spurious waves in supersonic solutions.

REFERENCES

1. Bristow, D. R.: A New Surface Singularity Method for Multi-Element Airfoil Analysis and Design. AIAA Paper 76-20, January 1976.

2. Maskew, B.; and Woodward, F. A.: Symmetrical Singularity Model for Lifting Potential Flow Analysis. AIAA Journal of Aircraft, Vol. 13, No. 9, September 1976, pp 733-734.

3. Woodward, F. A.; and Landrum, E. J.: The Supersonic Triplet - A New Aerodynamic Panel Singularity with Directional Properties. AIAA Paper 79-0273, 1979.

4. Morino, Luigi; and Kuo, Ching-Chiang: Subsonic Potential Aerodynamics for Complex Configurations: A General Theory. AIAA Journal, Vol. 12, No. 2, February 1974, pp. 191-197.

5. Bristow, D. R.; and Grose, G. G.: Modifications of the Douglas Neumann Program to Improve the Efficiency of Predicting Component Interference and High Lift Characteristics. NASA CR 3020, August 1978.

6. Ehlers, F. E.; Epton, M. A.; Johnson, F. T.; Magnus, A. E.; and Rubbert, P. E.: A Higher Order Panel Method for Linearized Supersonic Flow. NASA CR 3062, 1979.

7. Hess, John L.: Higher-Order Numerical Solutions of the Integral Equation for the Two-Dimensional Neumann Problem. Computer Methods in Applied Mechanics and Engineering, Vol. 2, No. 1, February 1973, pp. 1-15.

8. Hess, John L.: Analytic Solutions for Potential Flow Over a Class of Semi-Infinite Two-Dimensional Bodies Having Circular-Arc Noses. J. Fluid Mech., Vol. 60, part 2, 1973, pp. 226-239.

9. McGhee, Robert J.; and Beasley, William D.: Low Speed Aerodynamic Characteristics of a 17-Percent Thick Airfoil Section Designed for General Aviation Applications. NASA TN D-7428, 1973.

10. Bauer, F.; Garabedian, P.; and Korn, D.: Supercritical Wing Sections III, Lecture Notes in Economics and Mathematical Systems, Vol. 150, Springer-Verlag, New York, 1977.

11. Eppler, Richard; and Somers, Dan M.: Low Speed Airfoil Design and Analysis. NASA Conference Publication 2045, 1978, pp. 73-99.

12. Spence, D. A.: The Lift Coefficient of a Thin, Jet-Flapped Wing. Proc. Roy. Soc. (London), Ser. A, Vol. 238, No. 1212, December 4, 1956, pp. 46-68.

TABLE I.- Relative tangential velocity error in vicinity of stagnation point of concave nose body.

Formulation			Relative error in V_T	
Panel	Loading	Continuity	Ref. 7	Present Study
Flat	Constant σ	—	-2.0	-2.0
Flat	Linear σ	σ	-1.2	
Curved	Constant σ	Slope	- .9	
Flat	Constant σ, γ	—		-.040*
Flat	Linear σ, γ	σ, γ		-.037
Flat	Linear σ, γ	Vector		.0023

*Iterative solution

Table II.- Average calculated axial velocity in closed end duct.

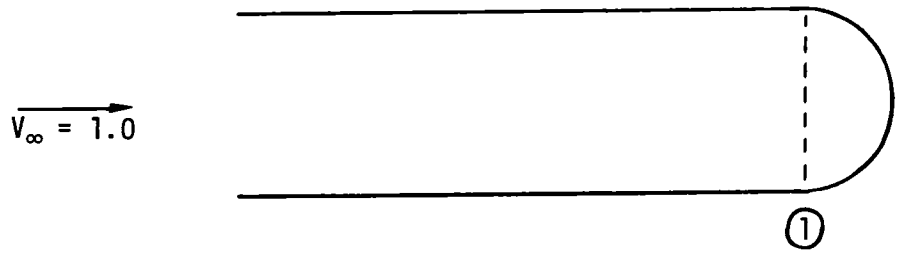

Formulation			Average axial velocity at station ①	
Panel	Loading	Continuity	Ref. 7	Present Study
Flat	Constant σ	—	.067	.072
Flat	Linear σ	σ	.069	
Curved	Constant σ	Slope	.0024	
Curved	Linear σ	σ, slope	.0015	
Curved	Quadratic σ	Higher order	.00081	
Flat	Constant σ, γ	—		0
Flat	Linear σ, γ	σ, γ		.0095
Flat	Linear σ, γ	Vector		0

Table III.- Variable area duct exit velocity errors.

Panel Loading	Continuity	Boundary Condition	Control Point Location	Constraint	Average Exit Velocity	Exit Velocity Error
Constant σ, γ	—	V_N or V_T	Midpanels	—	1.0700	.0700
Linear σ,γ	σ, γ	↓	↓	—	.9939	-.0061
↓	Vector			—	.9977	-.0023
	↓	$\Delta\phi = 0$	Midpanels	$\Sigma\gamma\ell = 0$	1.0864	.0864
		↓	Corners	$\Sigma\gamma\ell = 0$	.9446	-.0554
			Midpanels	$\Sigma\sigma\ell = 0$	.9918	-.0082
			Corners	$\Sigma\sigma\ell = 0$	.9923*	-.0077

*Solution slightly asymmetric

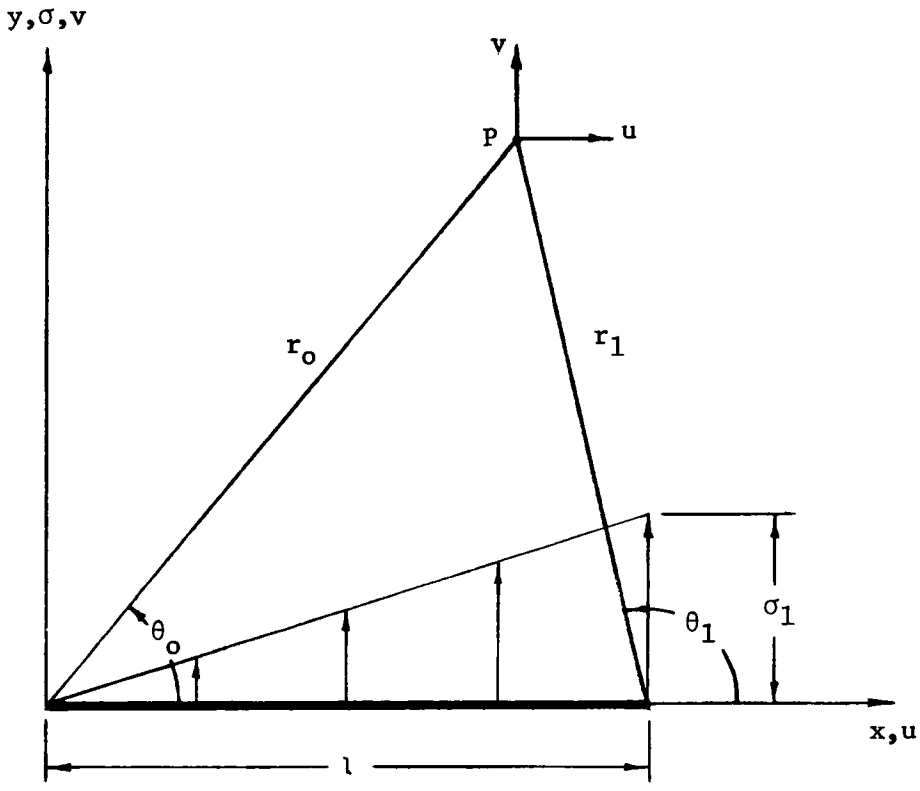

Figure 1.- Triangular source loading and induced velocities.

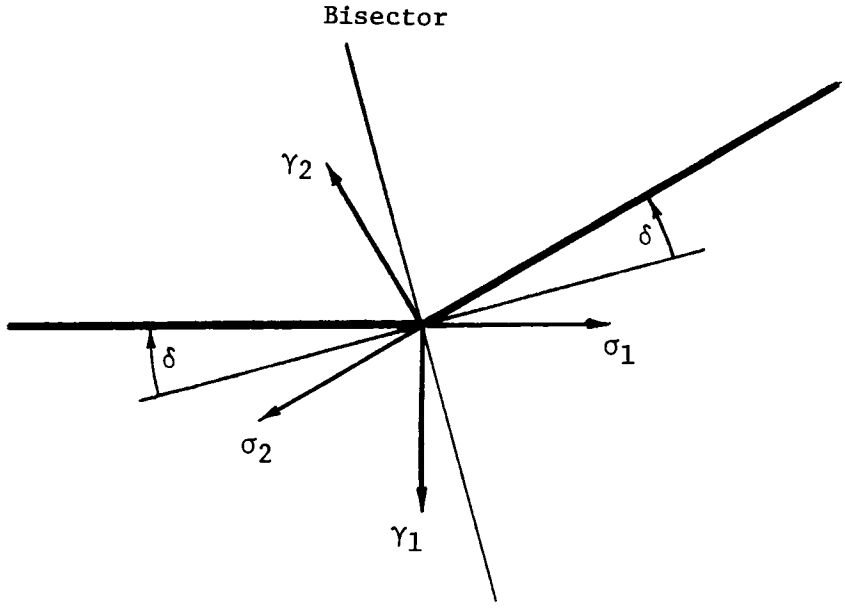

Figure 2.- Orientation of singular velocities.

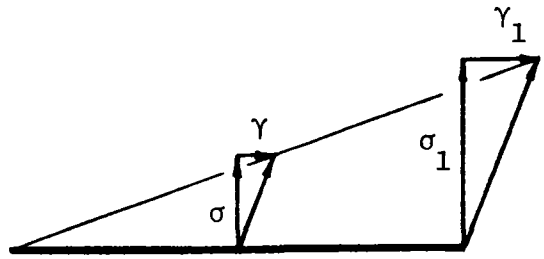

(a) Triangular combined loading

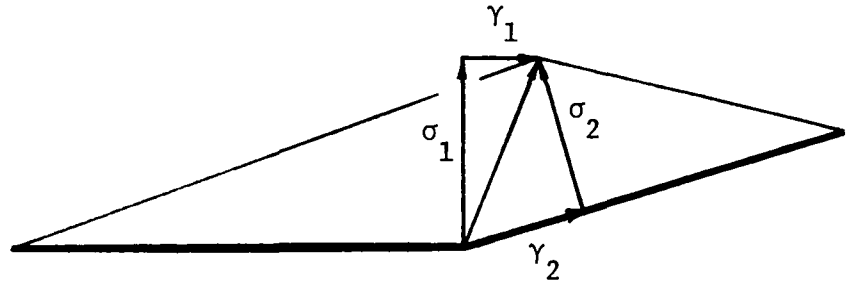

(b) Loading vector continuity

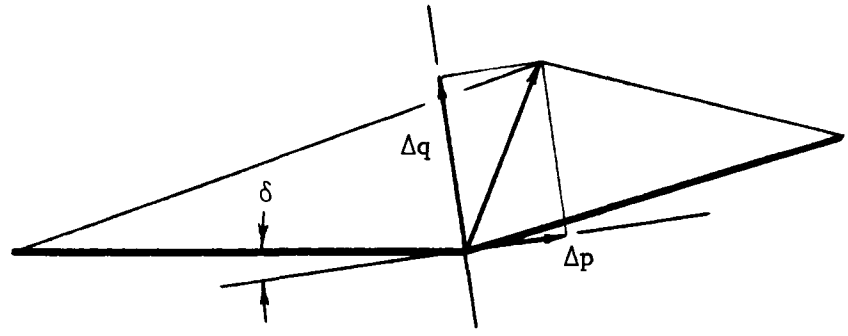

(c) Loading vector quantification

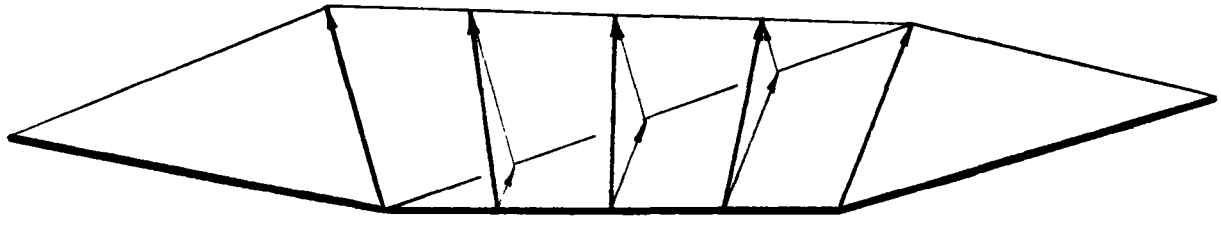

(d) Overlapping loading elements

Figure 3.- Properties of the vector-continuous loading element.

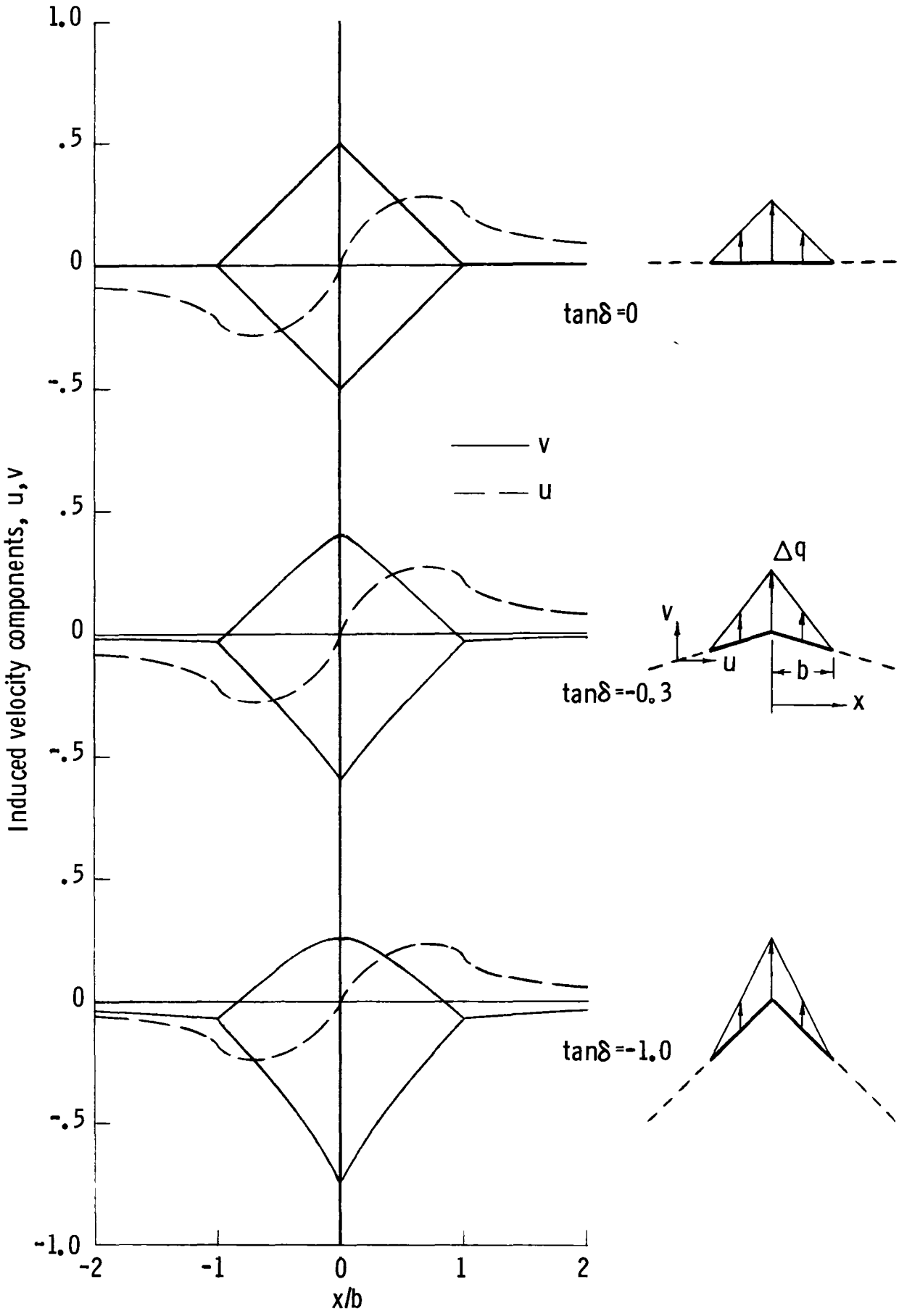

(a) Vector-continuous Δq loading

Figure 4.- Effect of dihedral angle on the self-induced velocities on the surfaces of a pair of intersecting panels with triangular loading.

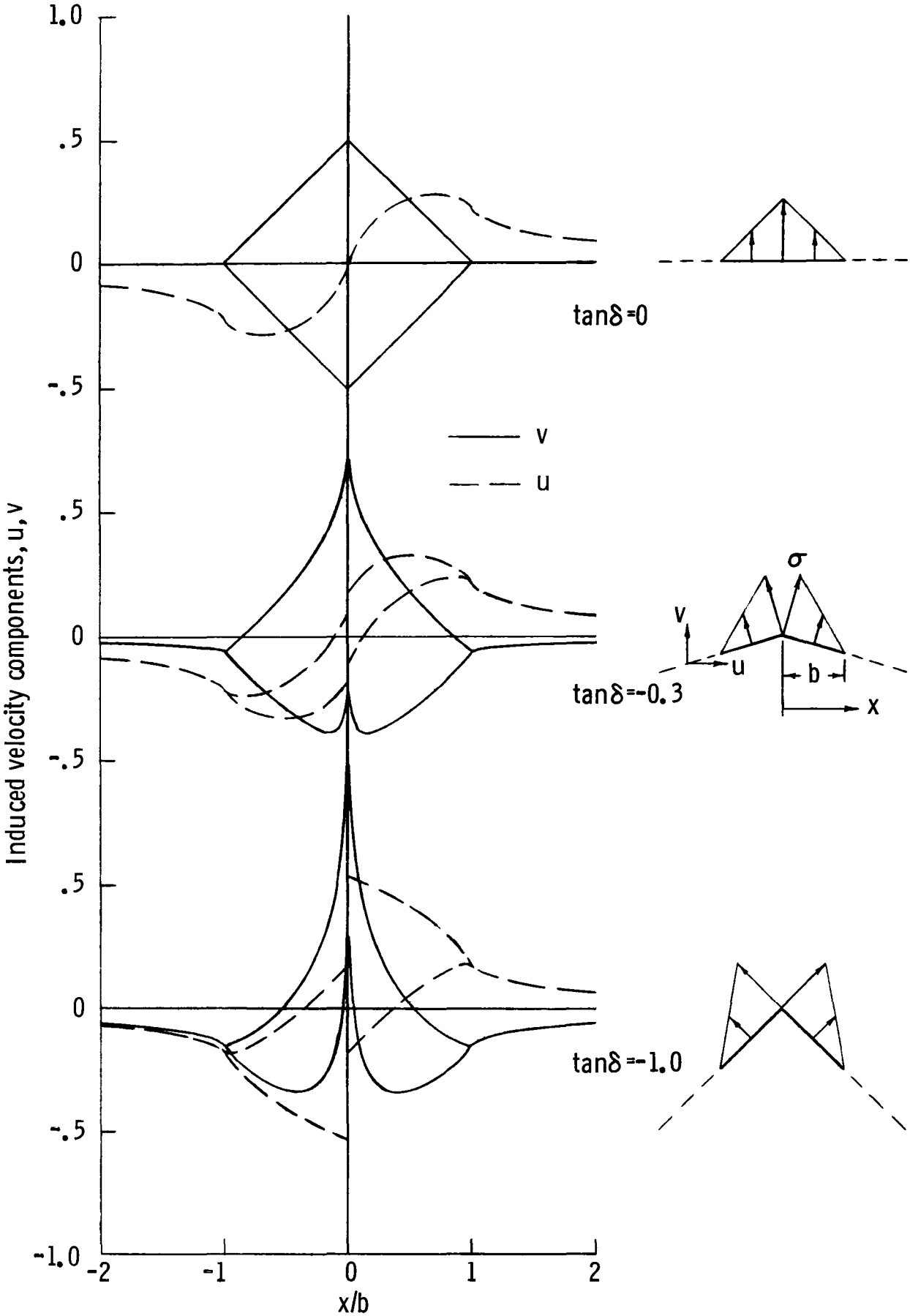

(b) Continuous source loading

Figure 4.- Concluded.

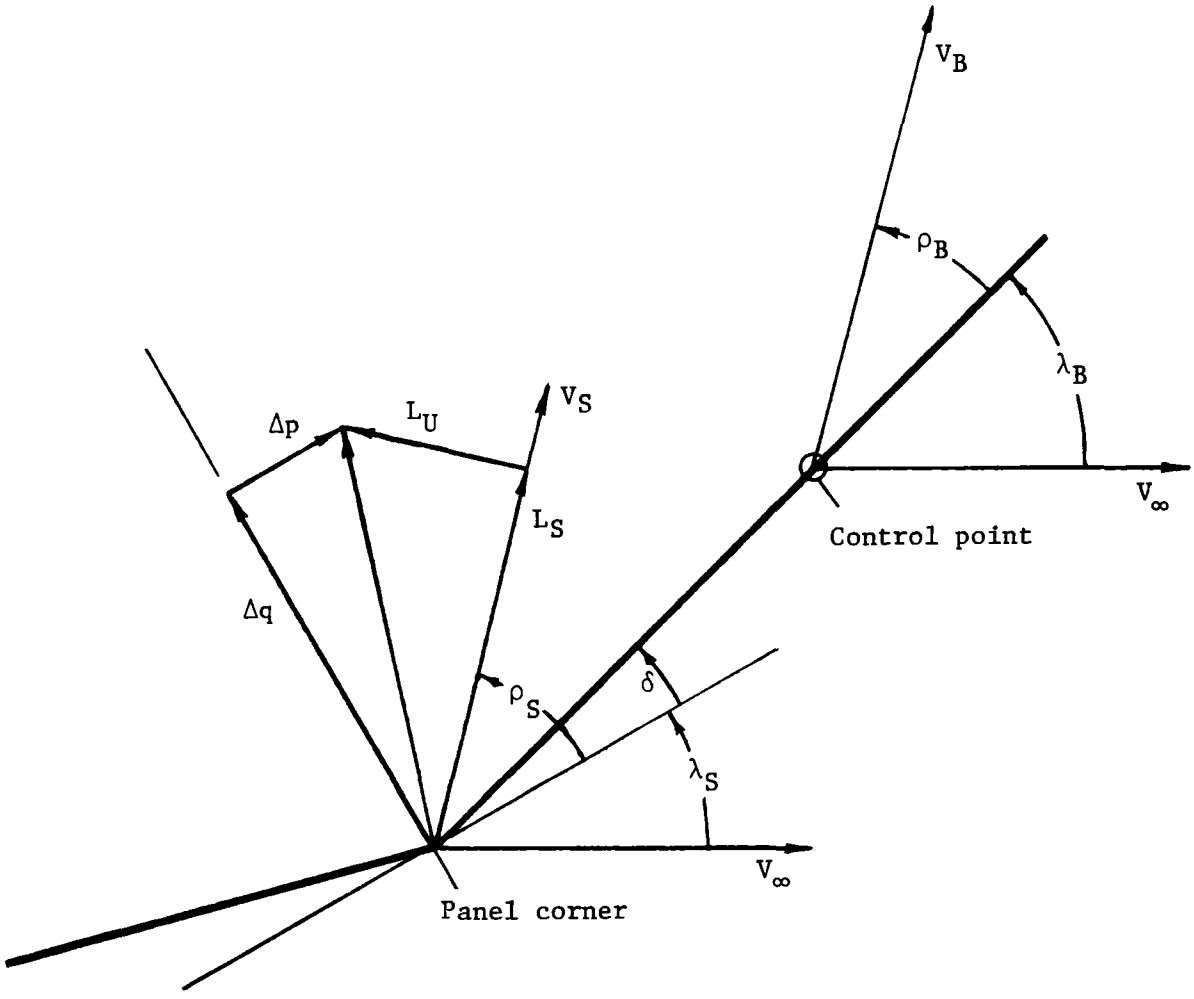

Figure 5.- Generalized boundary condition and loading specification.

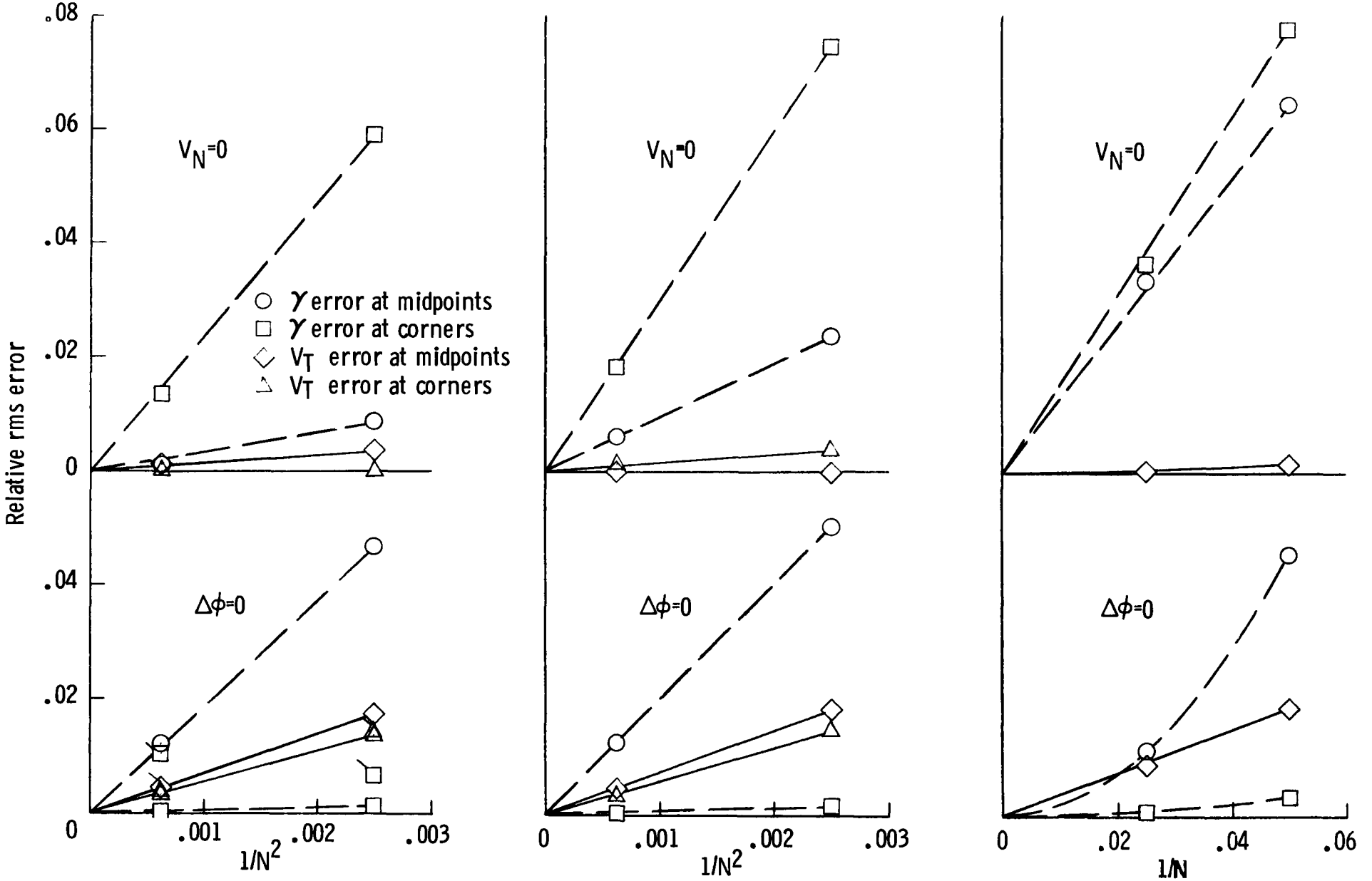

(a) Control points at panel corners, vector continuity

(b) Control points at panel midpoints, vector continuity

(c) Control points at panel midpoints, continuous σ and γ

Figure 6.- Discretization error trends in circular cylinder problem.

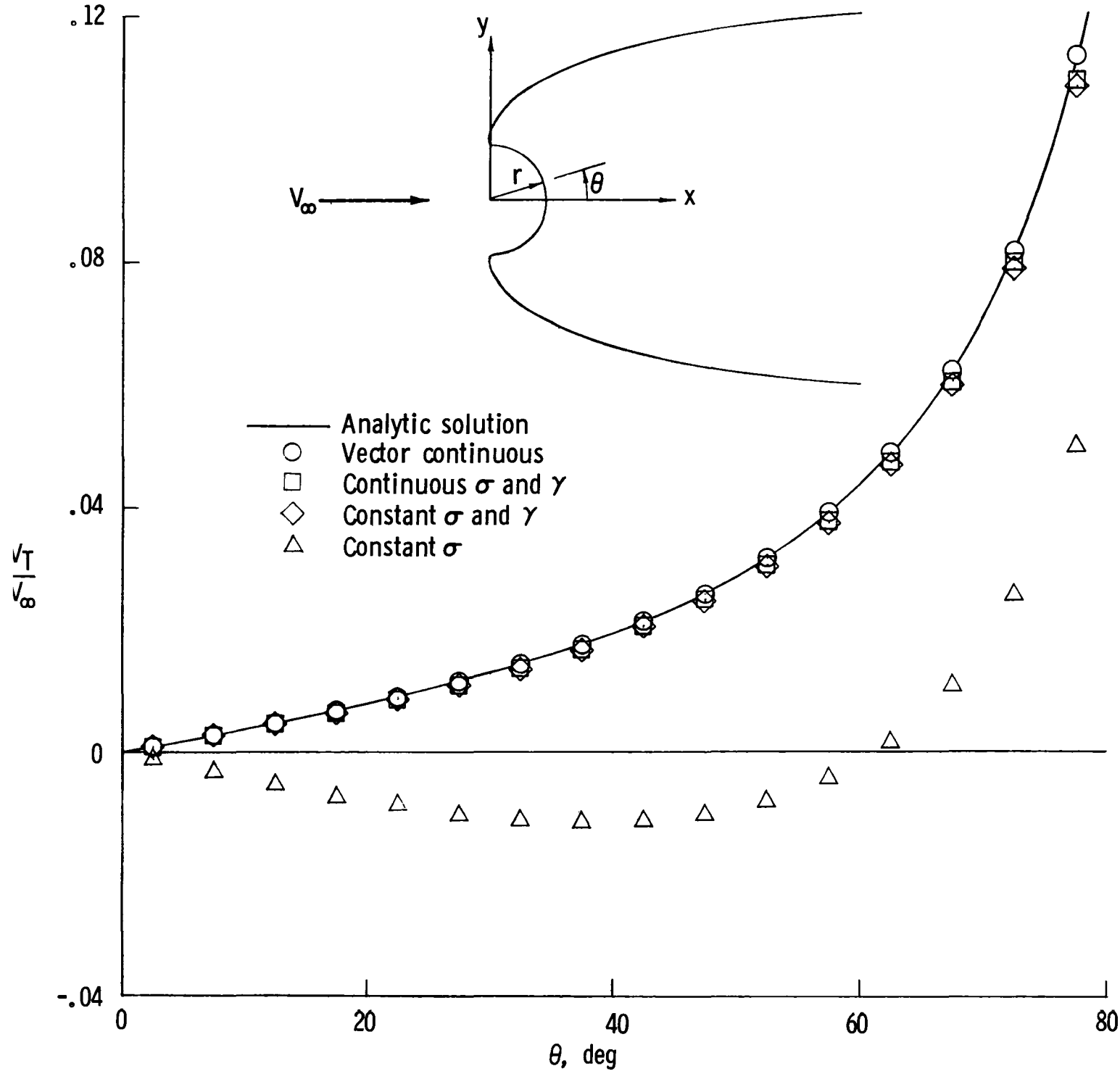

Figure 7.- Tangential velocity distribution in nose cavity of concave-nose body.

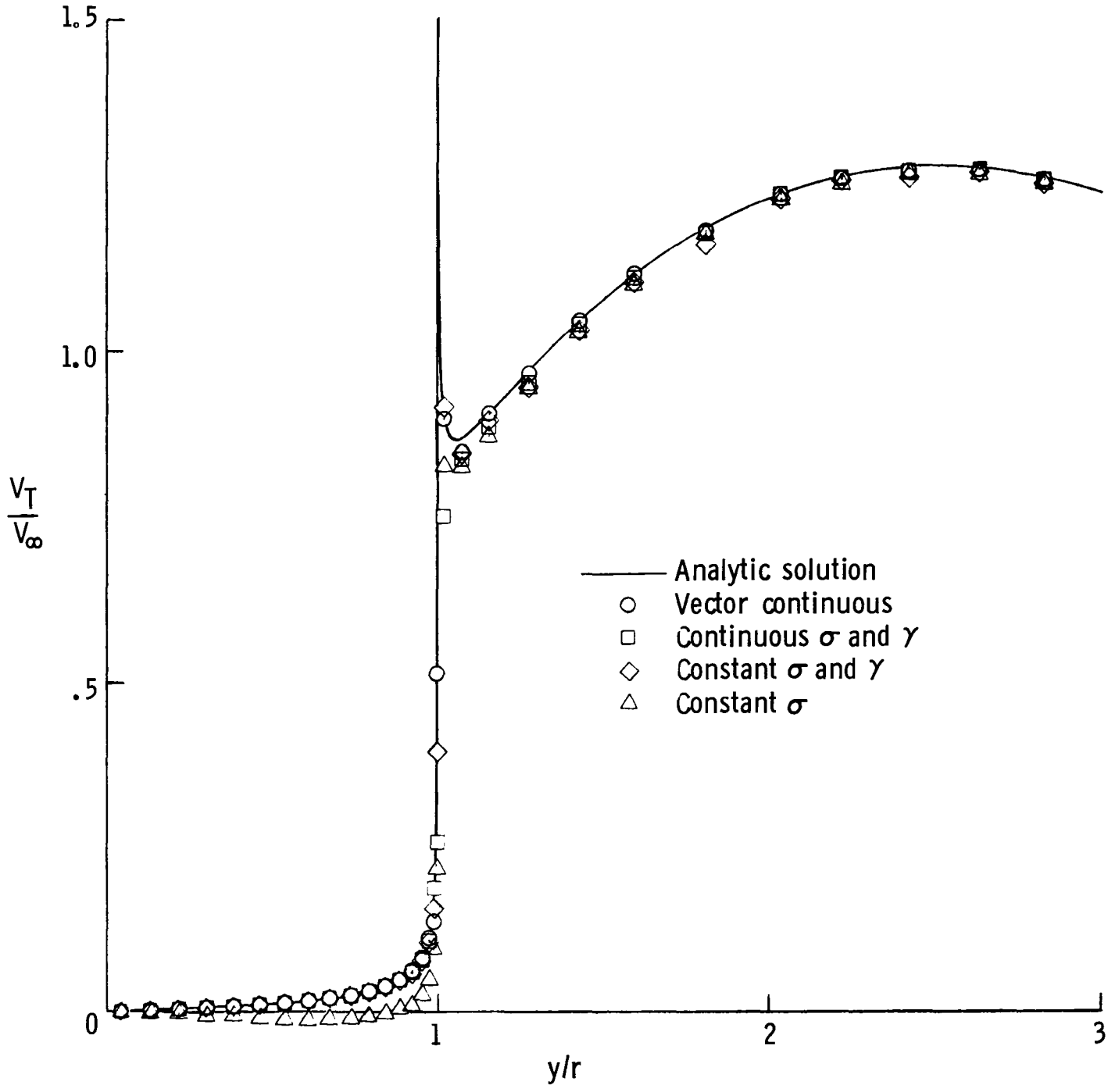

Figure 8.- Tangential velocity distribution over surface of concave-nose body.

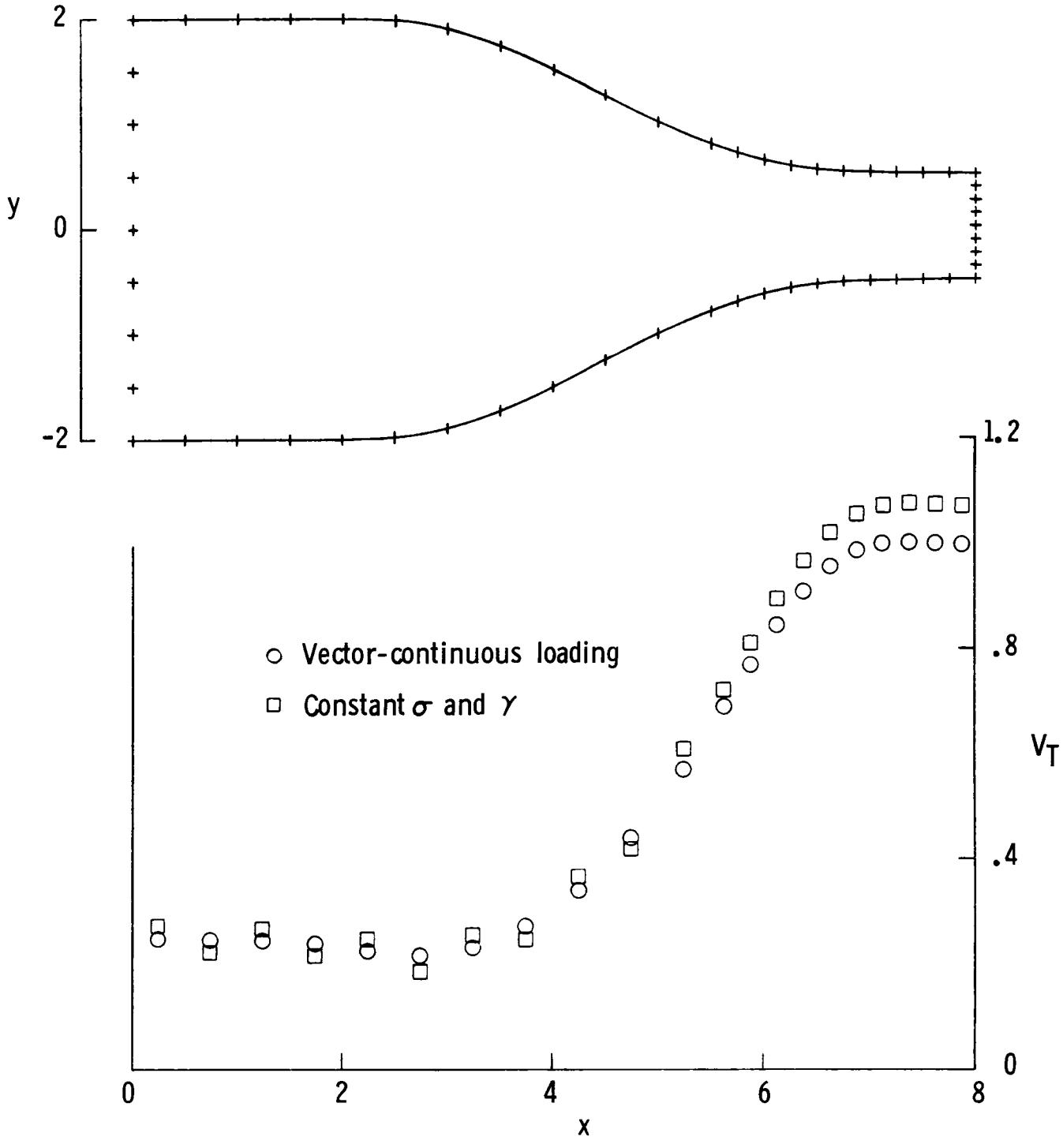

Figure 9.- Tangential velocity distribution on walls of variable area duct.

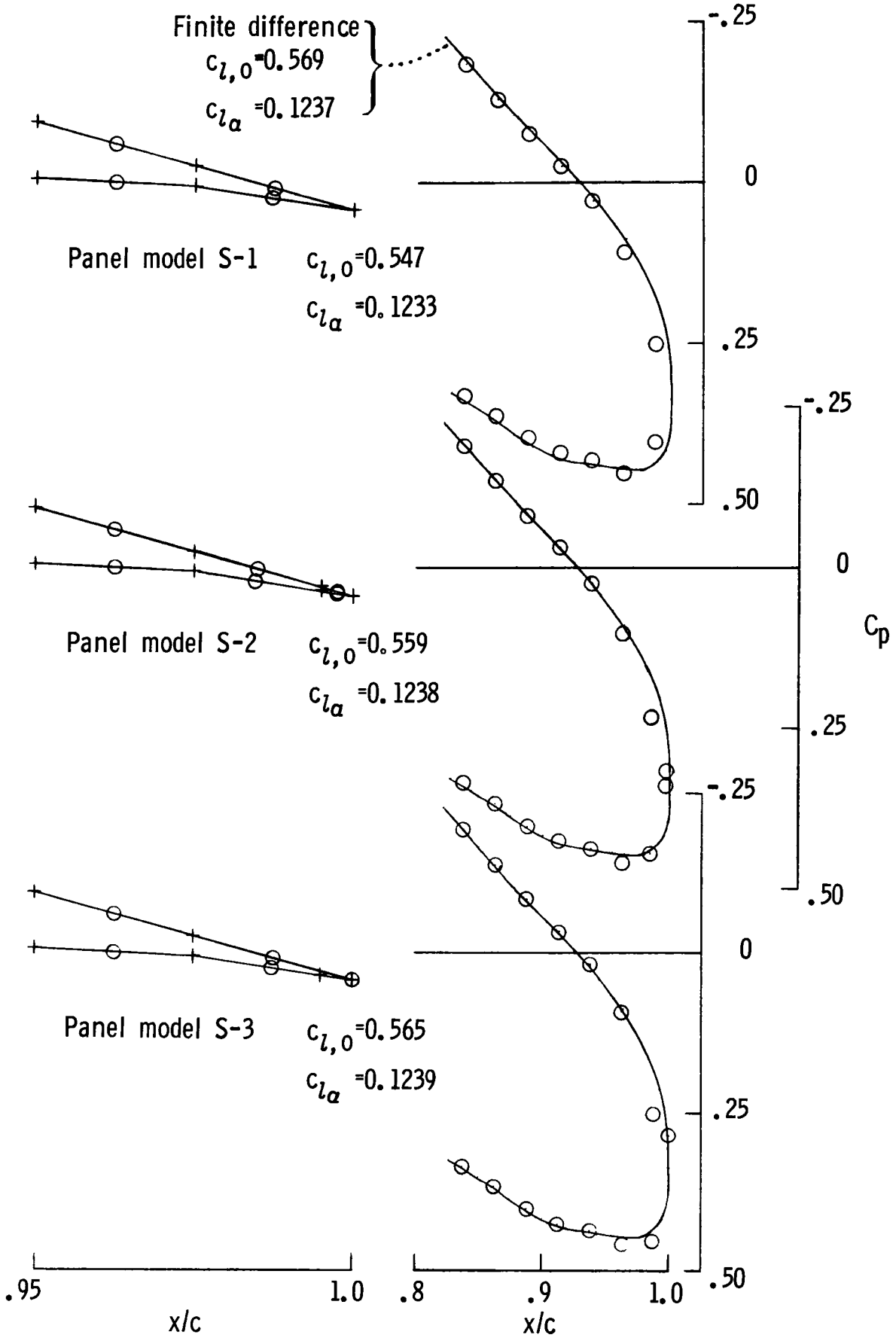

Figure 10.- Effect of trailing-edge paneling arrangement on the calculated lift and rear portion pressure distribution of a sharpened trailing-edge version of the NASA LS(1)-0417 airfoil section.

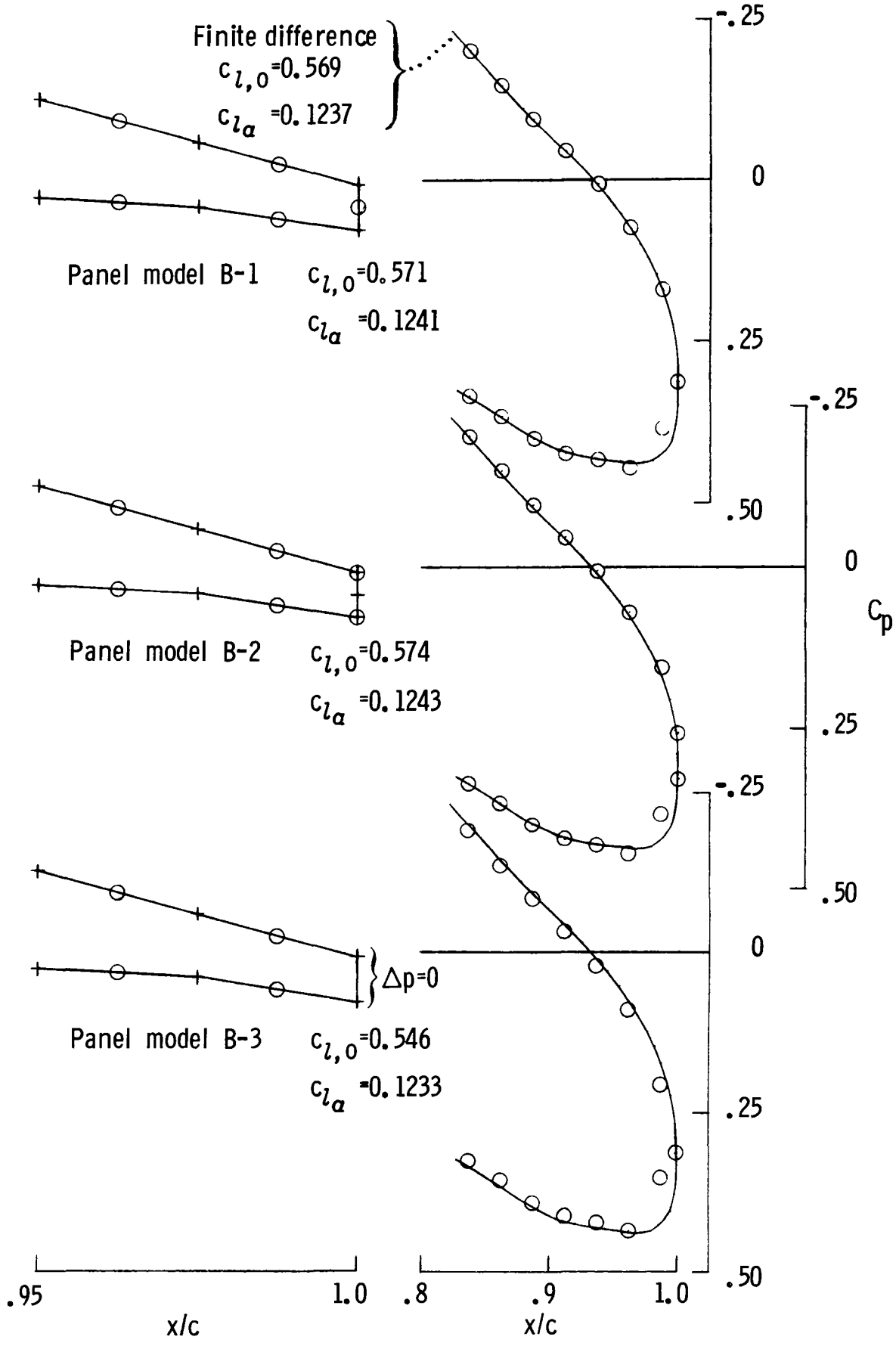

Figure 11.- Effect of trailing-edge paneling arrangement on the calculated lift and rear portion pressure distribution of the NASA LS(1)-0417 airfoil section.

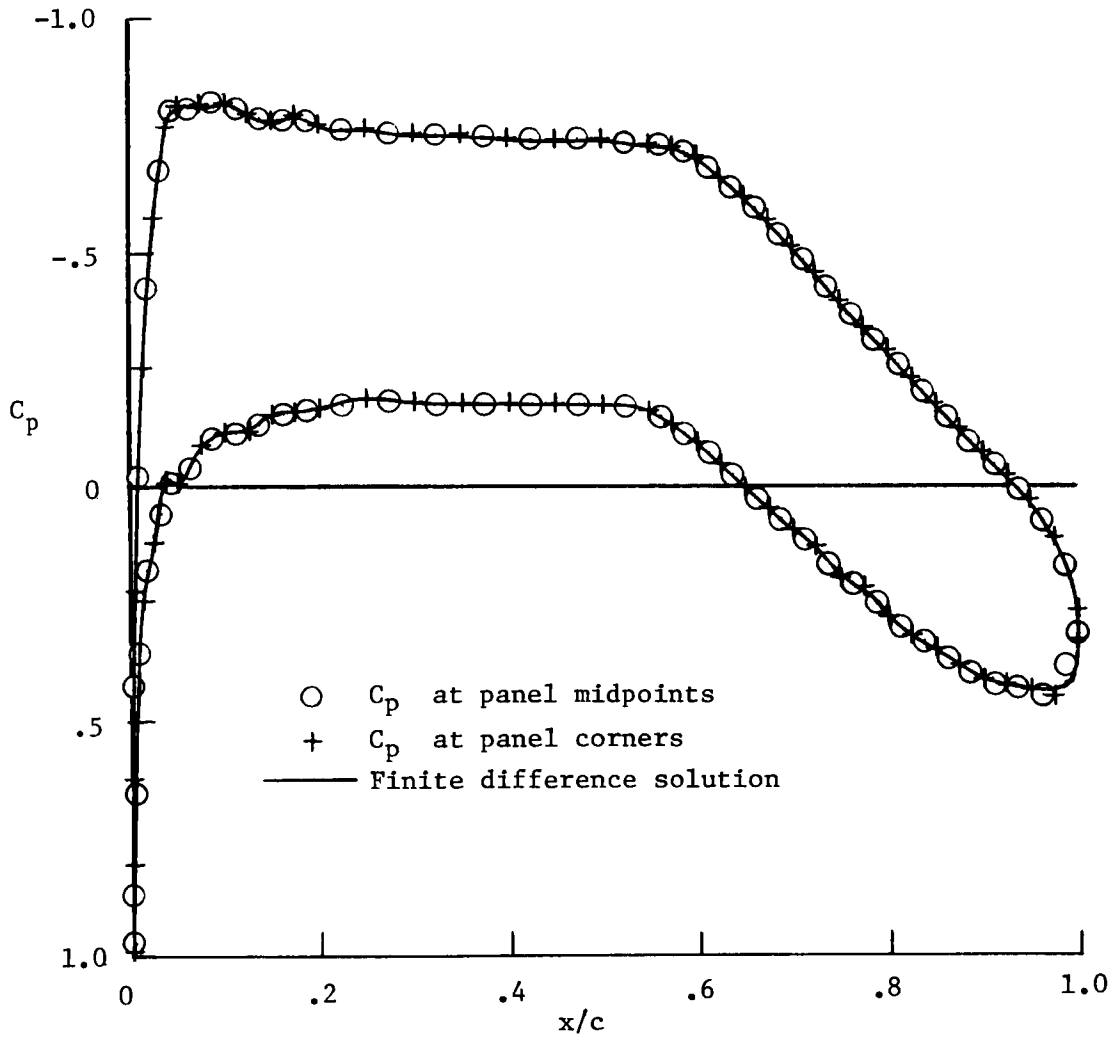

Figure 12.- Comparison of pressure distributions on the NASA LS(1)-0417 airfoil section calculated by the vector-continuous panel method and a finite different method, $\alpha=0°$.

End of Document